

Tree-level Interference in VBF production of Vh

Daniel Stolarski and Yongcheng Wu

Ottawa-Carleton Institute for Physics, Carleton University, 1125 Colonel By Drive, Ottawa, Ontario K1S 5B6, Canada

E-mail: stolar@physics.carleton.ca, ycwu@physics.carleton.ca

ABSTRACT: Vector boson scattering is a well known probe of electroweak symmetry breaking. Here we study a related process of two electroweak vector bosons scattering into a vector boson and a Higgs boson ($VV \rightarrow Vh, V = W, Z$). This process exhibits tree level interference and grows with energy if the Higgs couplings to electroweak bosons deviate from their Standard Model values. Therefore, this process is particularly sensitive to the relative sign of the ratio of the coupling between the Higgs and the W and Z , λ_{WZ} . In this work we show that a high energy lepton collider is well suited to study this process through vector boson fusion, estimate the potential sensitivity to this ratio, and show that a relatively modest amount of data can exclude $\lambda_{WZ} \simeq -1$.

Contents

1	Introduction	2
2	$2 \rightarrow 2$ Processes	4
3	VH production through VBF	6
4	Phenomenology Study	8
4.1	Total Rate Measurement	8
4.2	Differential Distributions Measurement	14
5	Summary	14

1 Introduction

In the Standard Model (SM), the Higgs boson is a necessary ingredient to keep longitudinal gauge boson scattering unitary at high energy [1–6]. Even in the presence of the Higgs, if its couplings deviate from those predicted by the SM, longitudinal gauge boson scattering will still grow with energy and new physics is needed to make the theory unitary [7–9]. Therefore, the experimental discovery of the Higgs [10, 11] is insufficient to probe the nature of the unitarization of longitudinal gauge boson scattering; detailed measurements of its couplings are necessary.

Vector boson scattering ($VV \rightarrow VV$, $V = Z, W$) is an extremely well studied subject (for a review see [12]). One can do a rotation in gauge space to study the similar process $VV \rightarrow hh$ [9], where h is the Higgs boson. More complicated processes involving gauge bosons can also be used to measure various Higgs couplings even when the Higgs is not one of the external particles [13]. In this work, we study another gauge rotated process:

$$VV \rightarrow Vh, \quad V = W, Z. \quad (1.1)$$

Like the two processes above, this one also exhibits growth with energy if the couplings of the Higgs to massive gauge bosons deviate from the Standard Model prediction. This process is especially sensitive to the ratio of the coupling of the Higgs to the W relative to that of the Z . In particular, if we define κ_W (κ_Z) as the deviation of the W (Z) coupling to the Higgs from the SM prediction ($\kappa_W = \kappa_Z = 1$ in the SM, see Eq. (2.2) below for more details), then we can define:

$$\lambda_{WZ} = \frac{\kappa_W}{\kappa_Z}, \quad (1.2)$$

as the specified ratio. The process in Eq. (1.1) exhibits *tree-level* interference effects between W and Z mediated processes, and the matrix element has a term that grows with energy proportional to $\lambda_{WZ} - 1$.

Because a heavy gauge boson collider is not feasible, the typical gauge boson scattering is studied experimentally via vector boson fusion (VBF), where W or Z 's are radiated off the initial state fermions and then scatter off one another. Analytic understanding can be further gained via the Effective W approximation [14–16], by treating the radiated gauge bosons as approximately on-shell. Gauge boson scattering has been observed at the LHC [17–20], but a lepton collider is a cleaner environment which may allow for more precise measurements. A lepton collider is a particularly good machine for precision studies of the Higgs, and planning has begun for several different machines including the ILC [21, 22], circular colliders CEPC [23] and FCC-ee [24, 25], and

CLIC [26, 27] which has higher Center of Mass (CM) energies, with designs ranging from 1.5 to 3 TeV.¹

Therefore, in this work we study the process of Eq. (1.1) with VBF at a high energy lepton collider:

$$\begin{aligned} e^+ e^- &\rightarrow \nu_e \bar{\nu}_e Z h, \\ e^+ e^- &\rightarrow \nu_e e W h. \end{aligned} \tag{1.3}$$

This process grows with the center of mass energy of the lepton collider, with CLIC being a particularly good machine for its study. As we will show, this process is very sensitive to modification of λ_{WZ} from the SM prediction because of the tree-level interference. The work here is complimentary to others that use interference effects to measure λ_{WZ} such as $e^+ e^- \rightarrow W^+ W^- h$ [29] or interference of tree and loop effects in $h \rightarrow 4\ell$ [30].

One particularly interesting scenario is that when λ_{WZ} is negative relative to the SM prediction. Tree-level processes without interference effects such as decays of $h \rightarrow ZZ^*$ [31, 32] and $h \rightarrow WW^*$ [33, 34] are only sensitive to $|\lambda_{WZ}|$. Fits to the couplings by the experimental collaborations [35–37] measure λ_{WZ} with approximately 10% precision but have almost no discriminating power between positive and negative values of λ_{WZ} .² The ultimate LHC sensitivity on this ratio is projected to be about 2% [38], but as far as we are aware, there has been no study on the sensitivity to the sign from rate measurements at the LHC. Negative values of λ_{WZ} can arise in models with scalars that have higher isospin representations [39] such as the Georgi-Machacek [40] model. In that case, however, the processes of Eq. (1.3) will be many times larger than the SM prediction and can be easily measured with a high energy lepton collider.

The remainder of this paper is structured as follows: in Section 2 we explore the behaviour of the $2 \rightarrow 2$ process focusing on the growth with energy, and in Section 3 we describe the process in vector boson fusion at a lepton collider and show the importance of tree-level interference. In Section 4 we conduct a phenomenological study including backgrounds and show how the analysis can be improved by taking differential distributions into account, and finally a summary is given in Section 5.

¹As this work was being completed, a study of this and other process at a high energy muon collider was posted in [28].

²The 13 TeV CMS analysis [36] actually has a best fit value that is negative, and the 13 TeV ATLAS analysis [37] does not consider negative values of λ_{WZ} .

2 2 → 2 Processes

We begin by analyzing the 2 → 2 processes

$$\begin{aligned} W^+ W^- &\rightarrow Z h, \\ W^\pm Z &\rightarrow W^\pm h, \end{aligned} \tag{2.1}$$

to understand the large interference effects that can occur. We parameterize the coupling of the Higgs (h) to the W and Z as

$$\mathcal{L} = h \left(\kappa_W g m_W W_\mu^+ W_\mu^- + \kappa_Z g \frac{m_Z^2}{2m_W} Z_\mu Z_\mu \right), \tag{2.2}$$

where g is the SM $SU(2)$ gauge coupling, and in the Standard Model $\kappa_W = \kappa_Z = 1$, with values away from one parameterizing deviation from the SM prediction.

Both processes in Eq. (2.1) have contributions from s and t -channel diagrams (the Feynman diagrams can be read from the VBF Feynman diagrams below in Fig. 2). In the first (second) process, the s -channel diagram is proportional to κ_Z (κ_W), while the t -channel diagrams are proportional to κ_W (κ_Z). We can divide the process into sub-processes based on the number of transversely vs. longitudinally polarized gauge bosons in this process. Direct calculation shows that the matrix elements with two or three longitudinal gauge bosons grows with energy. This is analogous to the classic studies of $WW \rightarrow WW$ scattering [1–6], and even though the s and t -channel processes individually grow with energy, their sum displays a cancellation such that the final amplitude does not grow with energy and the theory remains unitary at high energy. We summarize the high energy behaviour of the polarized matrix elements in Tab. 1 for different combinations of vector polarizations.

We can analyze the case $W_L W_L \rightarrow Z_L h$ in more detail. We expand the matrix elements for the s - and t -channel processes in the high energy limit:

$$\mathcal{M}_s (W_L^+ W_L^- \rightarrow Z_L h) = \frac{\kappa_Z g^2 \cos \theta}{4m_W^2} (s - m_h^2 + 2m_Z^2) + \mathcal{O}\left(\frac{1}{s}\right), \tag{2.3}$$

$$\begin{aligned} \mathcal{M}_t (W_L^+ W_L^- \rightarrow Z_L h) &= \frac{\kappa_W g^2}{4m_W^2} \left(\cos \theta (-s + 2m_W^2 + m_Z^2 - m_h^2) + 8m_W^2 \frac{\cos \theta}{\sin^2 \theta} \right) \\ &+ \mathcal{O}\left(\frac{1}{s}\right), \end{aligned} \tag{2.4}$$

where θ is the scattering angle in the centre of momentum frame. The singularity in the forward ($\theta = 0$) and backward ($\theta = \pi$) limits in the t -channel diagrams are artifacts

	$\mathcal{M}_{s/t}$	$d\sigma_{s/t}$	$\mathcal{M}_s + \mathcal{M}_t$	$d\sigma_{\text{tot}}$
TTT	$\frac{1}{\sqrt{s}}$	$\frac{1}{s^2}$	$\frac{1}{\sqrt{s}}$	$\frac{1}{s^2}$
LTT	s^0	$\frac{1}{s}$	s^0	$\frac{1}{s}$
LLT	\sqrt{s}	s^0	$\frac{1}{\sqrt{s}}$	$\frac{1}{s^2}$
LLL	s	s	s^0	$\frac{1}{s}$

Table 1. High energy behaviour of the polarized process given in Eq. (2.1) as a function of Mandelstam s for the matrix element \mathcal{M} and the differential cross section $d\sigma$. The first two columns are for the s - and t -channel processes individually, while the third and fourth columns are for the s - and t -channel processes summed. The different rows are for different combinations of polarizations of gauge bosons whether they are transverse (T) or longitudinal (L).

of the high energy expansion and are cut off by masses in the full expression. Adding the two matrix elements:

$$\mathcal{M}(W_L^+ W_L^- \rightarrow Z_L h) = \frac{g^2 \kappa_Z \cos \theta}{4m_W^2} (1 - \lambda_{WZ}) s + \mathcal{O}(s^0), \quad (2.5)$$

where λ_{WZ} is defined in Eq. (1.2) and equal to one in the SM. We see that at high energy, the SM predicts that the matrix element of this process goes to a constant, and thus cross section falls, preserving unitarity. On the other hand, if there is new physics that modifies the ratio of the coupling of the Higgs to the electroweak gauge bosons, $\lambda_{WZ} \neq 1$, then this amplitude and thus the cross section will grow quadratically with center of mass energy. This growth will eventually be cut off by new resonances or other effects of new physics. A particularly interesting case is that of $\lambda_{WZ} \simeq -1$. This is impossible to distinguish from the Standard model prediction without an interference measurement, and the process studied here is extremely sensitive to this scenario.

We now look at a full calculation of the cross section in Fig. 1. On the left panel, looking first at the solid lines which are the SM prediction, the cross section is dominated by the process with two transverse and one longitudinal gauge boson (LTT)³. Of these, the largest are the processes where one of the initial states is longitudinal, and the two transversely polarized gauge bosons have opposite chirality. If we now turn to the dashed lines which have $\lambda_{WZ} = -1$, we see the dramatic growth with energy of the

³Note that, the energy dependence of the cross section in LTT and LLL configurations does not behave as expected shown in Tab. 1. This is mainly due to the fact that in the forward and backward region ($\cos \theta = \pm 1$), the high energy expansion is different. When integrating over $\cos \theta$, we will obtain different dependence on the scattering energy. However, the overall cancellation between s and t/u contributions is not ruined.

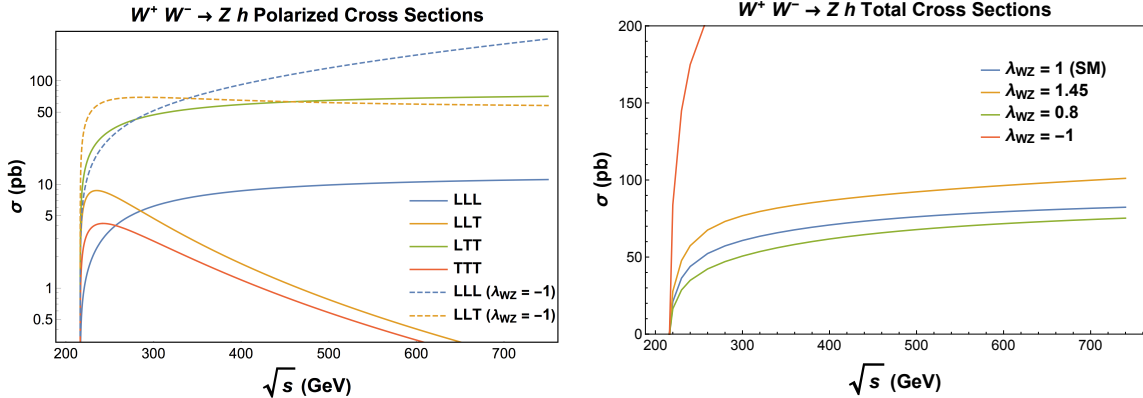


Figure 1. Left: Polarized cross sections of the process $W^+W^- \rightarrow Zh$ as a function of center of mass energy \sqrt{s} categorized by the number of transverse (T) or longitudinally (L) polarized vectors in the process. The solid lines are SM results while the dashed lines have $\lambda_{WZ} = -1$. **Right:** Total cross sections for the same process. The blue line is the SM result, while other lines have different values of λ_{WZ} . We have taken $\kappa_W = 1$ in all cases. Note that the left plot is on a log-scale, while the right one is linear.

process with all longitudinal gauge bosons, confirming the analysis of Eq. (2.5). We can also see that the process with two longitudinal gauge bosons is significantly enhanced.

On the right panel of Fig. 1 we study how the total cross section as a function of energy varies with λ_{WZ} , and we can again see that for $\lambda_{WZ} \simeq -1$, the cross section is much larger than the SM prediction for all energies. Even for moderate modifications of λ_{WZ} there can be significant changes to the cross section. Analyzing the isospin related processes $W^\pm Z \rightarrow W^\pm h$ gives analogous results. Therefore we see that because of the two processes that grow with energy, and the cancellation that occurs only at the SM value of λ_{WZ} , measurement of this process is a very sensitive probe of this coupling ratio. Unfortunately, an electroweak gauge boson collider is not feasible, so directly measuring these processes is not possible. In what follows we turn to the more realistic case of measuring vector boson scattering as a subprocess in a lepton collider.

3 VH production through VBF

The processes we are considering is the V +Higgs ($V = W, Z$) production through VBF at a Lepton Collider⁴:

$$e^+ e^- \rightarrow \nu_e \bar{\nu}_e Z h, \quad (3.1)$$

⁴We use electrons for the initial state, but the analysis is very similar at a muon collider.

$$e^+ e^- \rightarrow \nu_e e W h. \quad (3.2)$$

The main Feynman diagrams for these two processes are shown in Fig. 2. Fig. 2(a,b,d,f) contain the hWW vertex, while Fig. 2(c,e) rely on the hZZ vertex. The cross section as a function of collision energy for three different polarizations are also shown in Fig. 3. (For the cross section calculation, we require $p_T^\ell > 5$ GeV and $|\eta_\ell| < 3.5$.) The cross section grows as the collision energy increases. To fully utilize the potential of these two processes, we will consider both the 3 TeV and 1.5 TeV scenarios at CLIC [27]. We also note that polarization of the electron beam can significantly increase the cross section in the left-handed configuration.

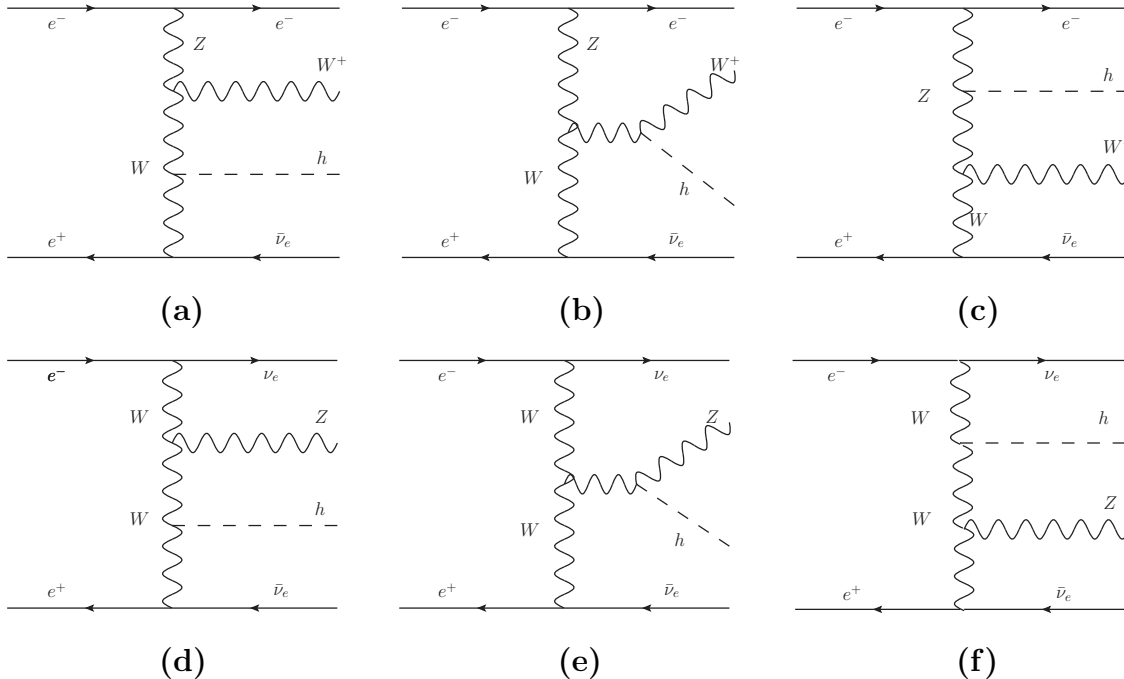


Figure 2. The Feynman Diagrams for Wh (a,b,c) and Zh (d,e,f) production through VBF processes at Lepton Collider.

We denote the contribution of the matrix element square from hWW couplings as $|\mathcal{M}_W|^2$ (e.g. from (a,b) or (d,f) only), the contribution from hZZ couplings as $|\mathcal{M}_Z|^2$ (from (c) or (e) only) and the interference term as \mathcal{M}_{WZ}^2 . Then the total matrix element square for either Wh or Zh processes can be written as (with the dependence on the κ of relevant couplings):

$$|\mathcal{M}|^2 = \kappa_W^2 |\mathcal{M}_W|^2 + \kappa_W \kappa_Z \mathcal{M}_{WZ}^2 + \kappa_Z^2 |\mathcal{M}_Z|^2. \quad (3.3)$$

The total cross section is

$$\sigma = \kappa_W^2 \sigma_W + \kappa_W \kappa_Z \sigma_{WZ} + \kappa_Z^2 \sigma_Z. \quad (3.4)$$

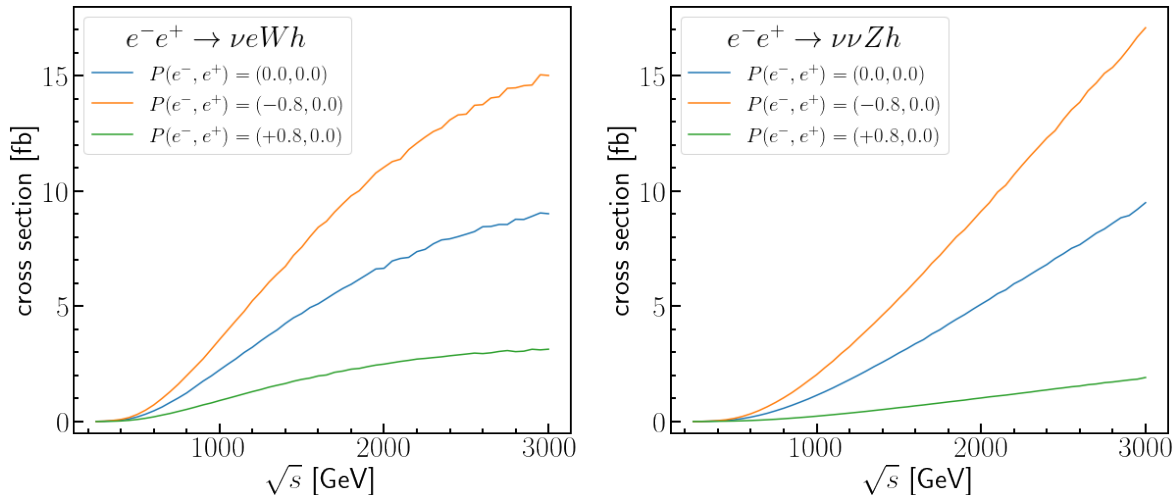


Figure 3. The cross section of two processes as a function of \sqrt{s} for three different polarizations. The cross sections are calculated using `MadGraph5_aMC@NLO` [41] with $p_T^\ell > 10$ GeV and $|\eta^\ell| < 3.5$.

Following the polarization configuration presented in [27], the individual contributions are listed in Tab. 2 for three different \sqrt{s} . We find that, besides the case $\sqrt{s} = 350$ GeV where the production rate is small, the interference effect is very large, comparable or even larger than the individual contributions of σ_W and σ_Z . This significant interference effect offers the opportunity to measure the κ_W , κ_Z as well as λ_{WZ} precisely. It also demonstrates the dramatic sensitivity to the sign of λ_{WZ} . In the following section, we conduct a detailed phenomenological study of this channel including backgrounds and realistic experimental cuts.

4 Phenomenology Study

A measurement of the cross section of the processes studied here can be translated into a measurement of λ_{WZ} . This process is particularly sensitive to the sign of this parameter because of the tree-level interference, and can thus relatively easily rule out the case with $\lambda_{WZ} < 0$ where the destructive interference effect in the SM turns into a constructive effect. Here we perform a realistic study of this cross section measurement.

4.1 Total Rate Measurement

The signal processes we consider are

$$e^- e^+ \rightarrow e^\pm \nu_e W^\mp h, \quad (4.1a)$$

σ [fb]		Wh		Zh	
\sqrt{s} [GeV]		$P(e^-) = -80\%$	$P(e^-) = 80\%$	$P(e^-) = -80\%$	$P(e^-) = 80\%$
350	σ_Z	6.81×10^{-3}	2.46×10^{-3}	1.08×10^{-2}	2.91×10^{-3}
	σ_W	3.85×10^{-2}	8.27×10^{-2}	1.49×10^{-2}	1.65×10^{-3}
	σ_{WZ}	-3.94×10^{-3}	-2.22×10^{-3}	-1.03×10^{-2}	-1.16×10^{-3}
1500	σ_Z	8.25×10^0	3.18×10^0	3.85×10^0	4.25×10^{-1}
	σ_W	1.22×10^1	4.11×10^0	6.85×10^0	7.66×10^{-1}
	σ_{WZ}	-1.28×10^1	-5.46×10^0	-5.38×10^0	5.93×10^{-1}
3000	σ_Z	3.51×10^1	1.34×10^1	1.87×10^1	2.09×10^0
	σ_W	4.31×10^1	1.50×10^1	2.97×10^1	3.27×10^0
	σ_{WZ}	-6.32×10^1	-2.52×10^1	-3.13×10^1	-3.45×10^0

Table 2. The individual contributions to total cross section for Wh and Zh VBF processes at different collision energies and different polarizations. The cross section is obtained from MadGraph5_aMC@NLO with cuts: $p_T^\ell > 10$ GeV and $|\eta_\ell| < 3.5$. The polarization configuration is following those in [27].

$$e^- e^+ \rightarrow \nu_e \bar{\nu}_e Z h. \quad (4.1b)$$

We consider the final state containing two isolated leptons, two b -jets (from Higgs decay) and \cancel{E}_T . Thus, the dominant backgrounds⁵ come from

$$e^- e^+ \rightarrow t\bar{t} \rightarrow b\bar{b}l^- l^+ \nu_\ell \bar{\nu}_\ell, \quad (4.2a)$$

$$e^- e^+ \rightarrow e^\pm \nu_e W^\pm Z \rightarrow e^\pm \nu_e \ell^\mp \nu_\ell b\bar{b}, \quad (4.2b)$$

$$e^- e^+ \rightarrow \nu_e \bar{\nu}_e ZZ \rightarrow \nu_e \bar{\nu}_e \ell^- l^+ b\bar{b}, \quad (4.2c)$$

$$e^- e^+ \rightarrow Zh, Z \rightarrow \ell^- l^+, h \rightarrow b\bar{b}, \quad (4.2d)$$

$$e^- e^+ \rightarrow ZW^+W^-, Z \rightarrow b\bar{b}, W^+ \rightarrow \ell^+ \nu_\ell, W^- \rightarrow \ell^- \bar{\nu}_\ell, \quad (4.2e)$$

$$e^- e^+ \rightarrow ZZZ, Z \rightarrow b\bar{b}, Z \rightarrow \ell^- l^+, Z \rightarrow \nu_\ell \bar{\nu}_\ell. \quad (4.2f)$$

The events are generated using MadGraph5_aMC@NLO [41] with PYTHIA8 [42] used for showering and hadronization. The detector effects are simulated with Delphes [43] using the CLIC card [44]. In order to improve the sensitivity, we simulate both 3 TeV and 1.5 TeV events with $P(e^-) = -0.8$ for the electron beam which are two scenarios for CLIC with 4000 and 2000 fb⁻¹ luminosity respectively [27].

⁵Another process with the same final states is associated production of a Higgs and two vector bosons, $e^- e^+ \rightarrow VVh$. This process also exhibits tree-level interference so it can be thought of as signal rather than background. The cross section is small and the topology is quite different from the signal, so it has a negligible contribution to this analysis after the cuts.

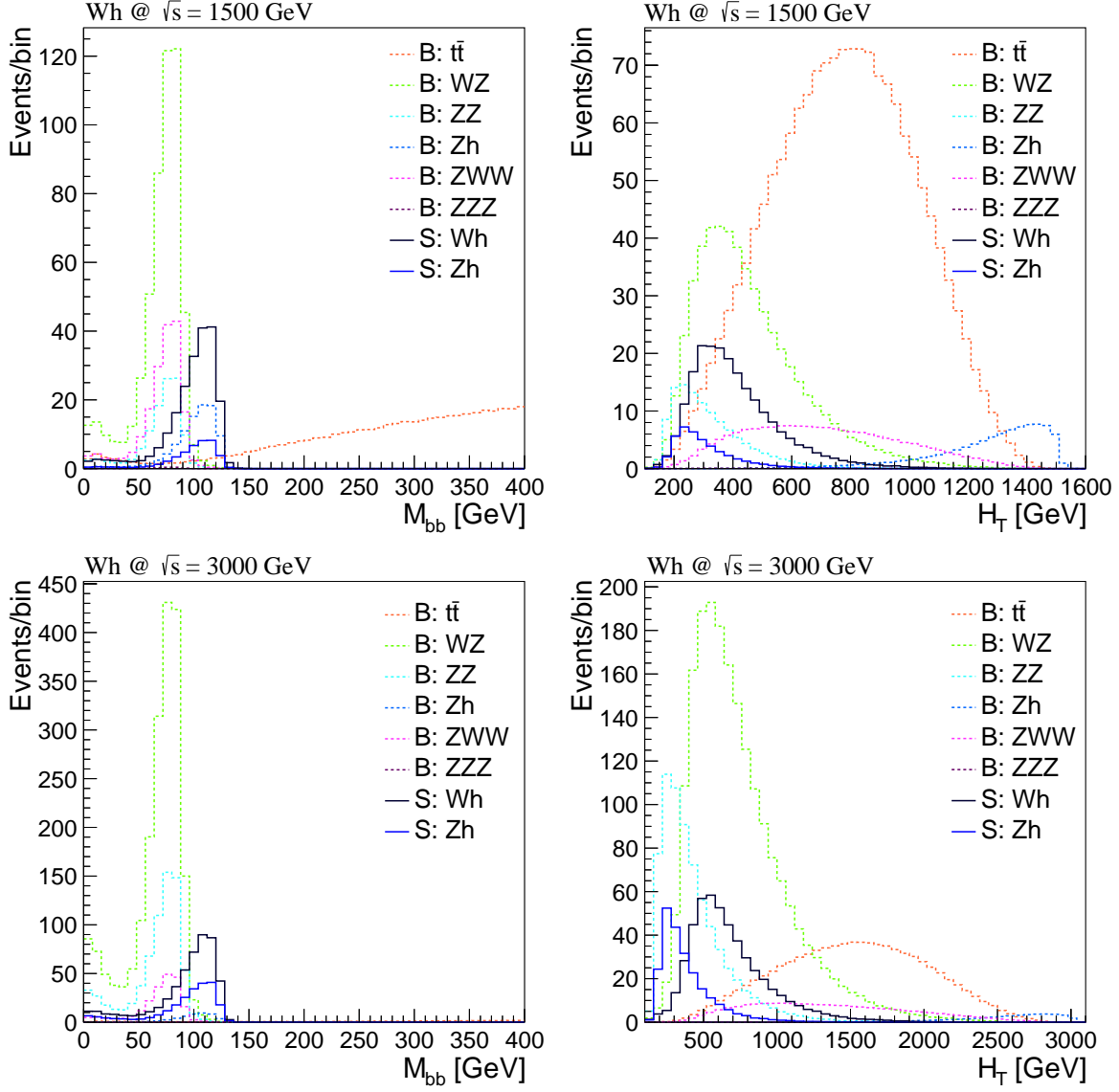


Figure 4. The distribution of m_{bb} and H_T in Wh channel at $\sqrt{s} = 1500$ GeV (Upper panels) and $\sqrt{s} = 3000$ GeV (Lower panels) with only the basic cuts listed in [Tab. 3](#) applied. Note that for $\sqrt{s} = 3000$ GeV the bulk of the m_{bb} distribution for the $t\bar{t}$ process is beyond the horizontal range of the plot.

The analysis is separated into two channels aiming on Wh and Zh production respectively. Based on the distributions and the event topology of the signal and background shown in [Fig. 4](#), the following cuts are applied on the events which are also listed in [Tab. 3](#):

- $p_T^\ell > 20$ GeV.
- $p_T^j > 20$ GeV.
- Two isolated leptons:
 - For Wh channel, at least one electron which directly comes from the beam remnants.
 - For Zh channel, one pair of opposite-sign same-flavor (OSSF) leptons is required.
- Two jets tagged as b -jet.
- The invariant mass of the two b -jet: $95 \text{ GeV} \leq m_{bb} \leq 130 \text{ GeV}$.
- The invariant mass of the two isolated leptons:
 - For Wh channel, $m_{\ell\ell} < 80 \text{ GeV}$ or $m_{\ell\ell} > 98 \text{ GeV}$.
 - For Zh channel, $75 \text{ GeV} < m_{\ell\ell} < 100 \text{ GeV}$.
- The scalar sum of transverse momenta of all reconstructed object:
 - For Wh channel:
$$\begin{cases} H_T \leq 2500 \text{ GeV} & \sqrt{s} = 3000 \text{ GeV}, \\ H_T \leq 1100 \text{ GeV} & \sqrt{s} = 1500 \text{ GeV}. \end{cases}$$
 - For Zh channel:
$$\begin{cases} H_T \leq 1500 \text{ GeV} & \sqrt{s} = 3000 \text{ GeV}, \\ H_T \leq 700 \text{ GeV} & \sqrt{s} = 1500 \text{ GeV}. \end{cases}$$

The cross sections for all processes after cuts are listed in [Tab. 4](#) for each channel, where in the last row, we also list the expected precision on the measurement of signal cross section with each channel assuming $\mathcal{L} = 4000 \text{ fb}^{-1}$ for $\sqrt{s} = 3000 \text{ GeV}$ and $\mathcal{L} = 2000 \text{ fb}^{-1}$ for $\sqrt{s} = 1500 \text{ GeV}$.

The numbers listed in [Tab. 4](#) are for $\kappa_W = 1$ and $\kappa_Z = 1$. By assuming that the selection efficiency will not change significantly for different values,⁶ we can obtain the events at any other values of κ_W and κ_Z by

$$\mathcal{N}_S(\kappa_W, \kappa_Z) = \mathcal{L} \times \sigma(\kappa_W, \kappa_Z) = \mathcal{L} \times \frac{\sigma^{\text{obs}}}{\sigma_0(\kappa_W = 1, \kappa_Z = 1)} \times \sigma_0(\kappa_W, \kappa_Z), \quad (4.3)$$

⁶This is a reasonable assumption, as we didn't use any selection cut that has direct dependence on the values of κ_W and κ_Z .

Cuts	Wh -Cuts	Zh -Cuts
Basic Cuts	$p_T^\ell > 20$ GeV, $N_\ell = 2$	
	$p_T^j > 20$ GeV, $N_b = 2$	
	$N_e \geq 1$	1 OSSF Pair
m_{bb}	95 GeV $\leq m_{bb} \leq 130$ GeV	
$m_{\ell\ell}$	$m_{\ell\ell} \leq 80$ GeV or $m_{\ell\ell} \geq 98$ GeV	75 GeV $\leq m_{\ell\ell} \leq 100$ GeV
H_T	$\begin{cases} H_T \leq 2500$ GeV & $\sqrt{s} = 3000$ GeV \\ $H_T \leq 1100$ GeV & $\sqrt{s} = 1500$ GeV \end{cases}	$\begin{cases} H_T \leq 1500$ GeV & $\sqrt{s} = 3000$ GeV \\ $H_T \leq 700$ GeV & $\sqrt{s} = 1500$ GeV \end{cases}

Table 3. The Cuts used for Wh channel and Zh channel.

σ (fb)		$\sqrt{s} = 3.0$ TeV, $\mathcal{L} = 4$ ab $^{-1}$			$\sqrt{s} = 1.5$ TeV $\mathcal{L} = 2$ ab $^{-1}$		
		Before Cuts	Wh -Cuts	Zh -Cuts	Before Cuts	Wh -Cuts	Zh -Cuts
Signal	$Wh(\text{VBF})$	1.97×10^0	7.26×10^{-2}	1.36×10^{-3}	9.62×10^{-1}	6.54×10^{-2}	2.37×10^{-3}
	$Zh(\text{VBF})$	6.47×10^{-1}	3.49×10^{-3}	7.21×10^{-2}	2.03×10^{-1}	1.30×10^{-3}	2.87×10^{-2}
BG	$t\bar{t}$	1.17×10^0	5.83×10^{-4}	6.10×10^{-6}	4.65×10^0	5.64×10^{-3}	8.05×10^{-5}
	$WZ(\text{VBF})$	4.47×10^0	9.97×10^{-3}	2.16×10^{-4}	1.84×10^0	5.86×10^{-3}	1.96×10^{-4}
	$ZZ(\text{VBF})$	1.92×10^0	4.21×10^{-4}	8.07×10^{-3}	5.92×10^{-1}	1.48×10^{-4}	2.88×10^{-3}
	Zh	5.88×10^{-2}	1.83×10^{-4}	4.15×10^{-4}	2.39×10^{-1}	4.10×10^{-4}	1.12×10^{-3}
	ZWW	4.01×10^{-1}	1.14×10^{-3}	4.97×10^{-6}	6.36×10^{-1}	2.02×10^{-3}	1.72×10^{-5}
	ZZZ	5.06×10^{-3}	6.04×10^{-7}	1.12×10^{-5}	9.79×10^{-3}	1.74×10^{-6}	2.34×10^{-5}
	Sum	8.02×10^0	1.23×10^{-2}	8.72×10^{-3}	7.97×10^0	1.41×10^{-2}	4.32×10^{-3}
	Precision (%)	6.18	6.17	Precision (%)	9.53	13.5	

Table 4. The cross sections of all signal and background (BG) processes (with final states $b\bar{b}\ell^+\ell^-$) at $\sqrt{s} = 1500, 3000$ GeV for $P(e^-) = -0.8$. Note that for the VBF processes, $p_T^\ell > 10$ GeV and $|\eta^\ell| < 3.5$ are imposed at the generation level for the forward/backward charged lepton. We also quote the the precision on the measurement of signal cross section that can be extracted with the given luminosity.

where $\sigma_0(\kappa_W, \kappa_Z)$ for Wh and Zh at $\sqrt{s} = 1500$ and 3000 GeV can be constructed from the data listed in [Tab. 2](#) as: $\sigma_0(\kappa_W, \kappa_Z) = \kappa_W^2 \sigma_W + \kappa_W \kappa_Z \sigma_{WZ} + \kappa_Z^2 \sigma_Z$. Then, assuming Poisson distribution for observed events, the negative log-likelihood (NLL) function is

$$\begin{aligned} \Delta\text{NLL}(\kappa_W, \kappa_Z) &= \text{NLL}(\kappa_W, \kappa_Z) - \text{NLL}_{\min} \\ &= \sum_i \left((\mathcal{N}_B^i + \mathcal{N}_S^i(1, 1)) \log \left[\frac{\mathcal{N}_B^i + \mathcal{N}_S^i(1, 1)}{\mathcal{N}_B^i + \mathcal{N}_S^i(\kappa_W, \kappa_Z)} \right] + \mathcal{N}_S^i(\kappa_W, \kappa_Z) - \mathcal{N}_S^i(1, 1) \right), \end{aligned} \quad (4.4)$$

where the summation runs over all the channels we have considered. Then the bound with an N - σ confidence interval corresponds to $\Delta\text{NLL} \leq N^2/2$.

Combining all these measurements, we can get the 68% (~ 1 - σ) and 95% (~ 2 - σ) confidence level (C.L.) region. The results are shown in [Fig. 5](#) in κ_W - κ_Z (left panel),

Benchmark	$\sqrt{s} = 3.0$ TeV	$\sqrt{s} = 1.5$ TeV
$\kappa_W = \pm 1, \kappa_Z = \mp 1$	3.4 fb^{-1}	14.1 fb^{-1}
$\kappa_W = 1, \kappa_Z = 0$	29.3 fb^{-1}	243.3 fb^{-1}
$\kappa_W = 0, \kappa_Z = 1$	62.1 fb^{-1}	1772.4 fb^{-1}

Table 5. The luminosity that is needed to exclude specific benchmark points at 95% C.L. against the SM case ($\kappa_W = 1$ and $\kappa_Z = 1$).

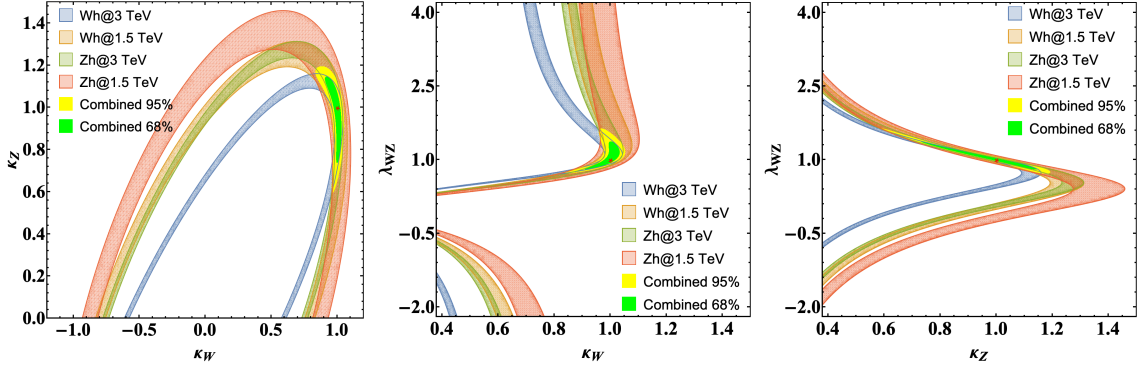


Figure 5. The constraints in the κ_W - κ_Z , κ_W - λ_{WZ} , and κ_Z - λ_{WZ} planes from the total rate measurements. We show the contours from the four different measurements at 68%, and also show the combined constraints at 68% C.L. (95% C.L.) in green (yellow). The SM values are indicated as red points.

κ_W - λ_{WZ} (middle panel) and κ_Z - λ_{WZ} (right panel) plane respectively. The 68% region for each individual channel is also given in each plot which shows the complementarity among these channels. Note that although we didn't optimize the cuts listed in [Tab. 3](#), they give a sensitivity very close to that achieved with a boosted decision tree using TMVA [\[45\]](#). This is because with these cuts or any relatively similar ones, the signal to background ratio is very high.

Besides the C.L. region around SM point shown in [Fig. 5](#), we can also estimate the luminosity that is needed to exclude some non-SM benchmark points. For this purpose, we will not combine $\sqrt{s} = 1.5$ TeV and 3.0 TeV, as each has its own luminosity. The results are shown in [Tab. 5](#), and we see that significantly less data than the standard proposals is required to exclude these scenarios. In particular, the scenario with $\lambda_{WZ} \simeq -1$, which is very difficult to probe in other processes, can be probed with just a few inverse femtobarns.

4.2 Differential Distributions Measurement

Because of the growth with energy described in [Section 2](#), the dependence of the matrix element on \hat{s} is different for s - and t/u -channels. Therefore, the s and t/u channels depend on κ_W and κ_Z differently. Hence, the differential distribution shape will shift for different value of λ_{WZ} . This is illustrated in [Fig. 6](#) in which we choose 3 different values of λ_{WZ} with $\kappa_W = 1$ and the distributions are all renormalized to 1. Note that we have generated sufficiently large Monte Carlo samples to suppress the statistical fluctuations. Thus, the difference in the shape of the distributions for different values of λ_{WZ} comes from the behaviour of the matrix element.

In order to estimate the discrimination power, the MC events (including both signal and backgrounds) are used to obtain the “observed” ($\kappa_W = 1$ and $\lambda_{WZ} = 1$) and “expected” (otherwise) distributions (shape) of $\sqrt{\hat{s}}$. The distributions as well as the total number of events are utilized to construct the extended likelihood by which we can determine the C.L. region for λ_{WZ} using similar method in previous section. The ΔNLL as a function of λ_{WZ} when $\kappa_W = 1$ is shown in [Fig. 7](#). We find that utilizing the $\sqrt{\hat{s}}$ distribution can significantly improve the sensitivity.

From [Fig. 7](#), we see that the sensitivity of the total measurement is particularly weak for $1 \lesssim \lambda_{WZ} \lesssim 1.5$. This is because for fixed κ_W as in [Fig. 7](#), we have from [Eq. \(3.4\)](#)

$$\frac{\partial\sigma}{\partial\lambda_{WZ}} \sim -\frac{\sigma_{WZ}}{\lambda_{WZ}^2} - \frac{2\sigma_Z}{\lambda_{WZ}^3}. \quad (4.5)$$

Looking at [Tab. 2](#), we see that in all four scenarios we are interested in, this derivative vanishes for λ_{WZ} between 1 and 1.5, so the cross section in that region is changing very slowly and there is little sensitivity. On the other hand, the differential cross section in $\sqrt{\hat{s}}$ will change with fewer events near threshold and more events at higher energy as we move away from $\lambda_{WZ} = 1$, allowing this analysis to break the approximate degeneracy in the total rate measurement.

5 Summary

The nature of electroweak symmetry breaking and whether the Higgs has the precise properties given in the Standard Model is still not fully explored by data. The couplings of the Higgs to heavy gauge bosons are a particularly important probe of the mechanism that gives mass to the W and Z . The ratio of those couplings, λ_{WZ} (see [Eq. \(1.2\)](#) and [Eq. \(2.2\)](#) for a precise definition) has been measured by the LHC to approximately 10% precision, but as yet we have essentially no information about the sign of λ_{WZ} .

Sign measurements are easiest in processes with tree-level interference; these processes will have very large deviations if the relative sign of a coupling is changed but the

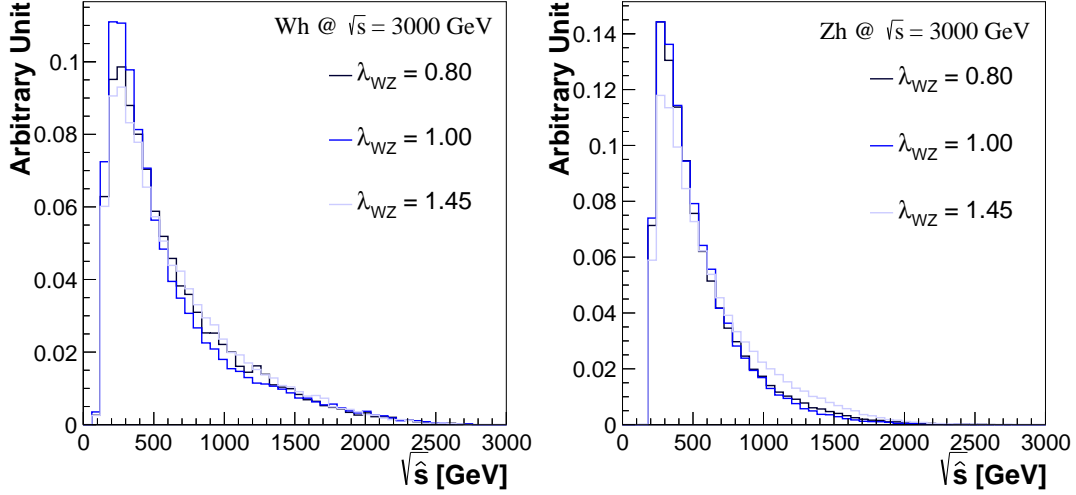


Figure 6. The differential distributions of \hat{s} for different values of λ_{WZ} for Wh (left) and Zh (right) channel at $\sqrt{s} = 3000$ GeV.

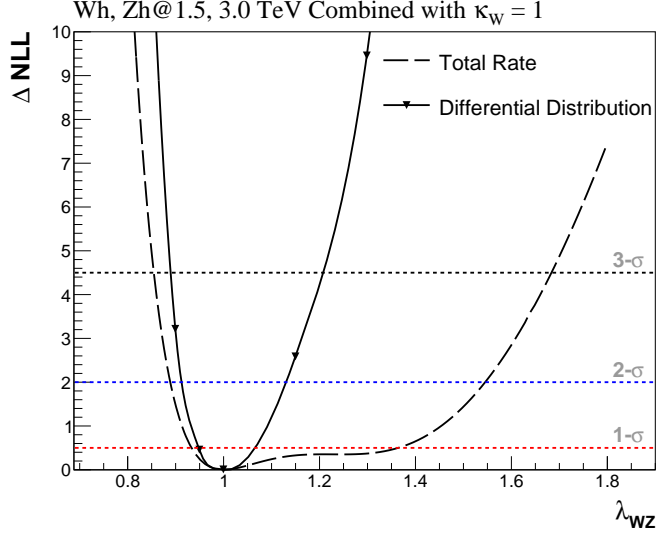


Figure 7. The ΔNLL (see text for definition) for different values of λ_{WZ} with $\kappa_W = 1$ combining all Wh and Zh channels at both 1.5 and 3.0 TeV CLIC.

magnitude is kept constant. In this work we have studied $VV \rightarrow Vh$, $V = W, Z$ using vector boson fusion at a high energy lepton collider. This process exhibits tree-level interference between diagrams proportional to the Higgs coupling to W and that to Z . If there is a deviation from the SM prediction of $\lambda_{WZ} = 1$, then this process exhibits growth with energy. Therefore, at high energy there will be very large destructive

interference between different processes as shown in [Tab. 2](#).

We have performed a study of this process at a potential future lepton collider with centre of mass energies of 1.5 and 3 TeV. With simple cuts, one can get a signal to background ratio well above one. We have shown that combining the $e^+ e^- \rightarrow \nu_e \bar{\nu}_e Z h$ and the $e^+ e^- \rightarrow \nu_e e W h$ channels as well as combining measurements at different center of mass energies, one can measure the couplings of the gauge bosons to the Higgs with a reasonable precision. As discussed above, this channel is particularly powerful at probing $\lambda_{WZ} \simeq -1$, which can be excluded with a small fraction of the expected data. Finally, we have shown that including the $\sqrt{\hat{s}}$ differential distribution can further improve the measurement.

Acknowledgments

We would like to thank Cheng-Wei Chiang for very useful discussions and communication. This work is supported in part by the Natural Sciences and Engineering Research Council of Canada (NSERC).

References

- [1] C. H. Llewellyn Smith, *High-Energy Behavior and Gauge Symmetry*, *Phys. Lett.* **46B** (1973) 233–236.
- [2] M. J. G. Veltman, *Second Threshold in Weak Interactions*, *Acta Phys. Polon.* **B8** (1977) 475.
- [3] B. W. Lee, C. Quigg, and H. B. Thacker, *The Strength of Weak Interactions at Very High-Energies and the Higgs Boson Mass*, *Phys. Rev. Lett.* **38** (1977) 883–885.
- [4] B. W. Lee, C. Quigg, and H. B. Thacker, *Weak Interactions at Very High-Energies: The Role of the Higgs Boson Mass*, *Phys. Rev.* **D16** (1977) 1519.
- [5] G. Passarino, *Large Masses, Unitarity and One Loop Corrections*, *Phys. Lett.* **156B** (1985) 231–235.
- [6] G. Passarino, *W W scattering and perturbative unitarity*, *Nucl. Phys.* **B343** (1990) 31–59.
- [7] J. M. Cornwall, D. N. Levin, and G. Tiktopoulos, *Derivation of Gauge Invariance from High-Energy Unitarity Bounds on the s Matrix*, *Phys. Rev.* **D10** (1974) 1145. [Erratum: *Phys. Rev.* **D11**, 972 (1975)].
- [8] G. F. Giudice, C. Grojean, A. Pomarol, and R. Rattazzi, *The Strongly-Interacting Light Higgs*, *JHEP* **06** (2007) 045, [[hep-ph/0703164](#)].

- [9] R. Contino, C. Grojean, M. Moretti, F. Piccinini, and R. Rattazzi, *Strong Double Higgs Production at the LHC*, *JHEP* **05** (2010) 089, [[arXiv:1002.1011](#)].
- [10] **ATLAS** Collaboration, G. Aad et al., *Observation of a new particle in the search for the Standard Model Higgs boson with the ATLAS detector at the LHC*, *Phys. Lett.* **B716** (2012) 1–29, [[arXiv:1207.7214](#)].
- [11] **CMS** Collaboration, S. Chatrchyan et al., *Observation of a New Boson at a Mass of 125 GeV with the CMS Experiment at the LHC*, *Phys. Lett.* **B716** (2012) 30–61, [[arXiv:1207.7235](#)].
- [12] M. Szleper, *The Higgs boson and the physics of WW scattering before and after Higgs discovery*, [arXiv:1412.8367](#).
- [13] B. Henning, D. Lombardo, M. Riemann, and F. Riva, *Measuring Higgs Couplings without Higgs Bosons*, *Phys. Rev. Lett.* **123** (2019), no. 18 181801, [[arXiv:1812.09299](#)].
- [14] S. Dawson, *The Effective W Approximation*, *Nucl. Phys.* **B249** (1985) 42–60.
- [15] Z. Kunszt and D. E. Soper, *On the Validity of the Effective W Approximation*, *Nucl. Phys.* **B296** (1988) 253–289.
- [16] P. Borel, R. Franceschini, R. Rattazzi, and A. Wulzer, *Probing the Scattering of Equivalent Electroweak Bosons*, *JHEP* **06** (2012) 122, [[arXiv:1202.1904](#)].
- [17] **CMS** Collaboration, A. M. Sirunyan et al., *Measurement of vector boson scattering and constraints on anomalous quartic couplings from events with four leptons and two jets in proton-proton collisions at $\sqrt{s} = 13$ TeV*, *Phys. Lett.* **B774** (2017) 682–705, [[arXiv:1708.02812](#)].
- [18] **CMS** Collaboration, A. M. Sirunyan et al., *Observation of electroweak production of same-sign W boson pairs in the two jet and two same-sign lepton final state in proton-proton collisions at $\sqrt{s} = 13$ TeV*, *Phys. Rev. Lett.* **120** (2018), no. 8 081801, [[arXiv:1709.05822](#)].
- [19] **ATLAS** Collaboration, M. Aaboud et al., *Observation of electroweak $W^\pm Z$ boson pair production in association with two jets in pp collisions at $\sqrt{s} = 13$ TeV with the ATLAS detector*, *Phys. Lett.* **B793** (2019) 469–492, [[arXiv:1812.09740](#)].
- [20] **ATLAS** Collaboration, M. Aaboud et al., *Observation of electroweak production of a same-sign W boson pair in association with two jets in pp collisions at $\sqrt{s} = 13$ TeV with the ATLAS detector*, *Phys. Rev. Lett.* **123** (2019), no. 16 161801, [[arXiv:1906.03203](#)].
- [21] **ILC** Collaboration, G. Aarons et al., *International Linear Collider Reference Design Report Volume 2: Physics at the ILC*, [arXiv:0709.1893](#).

- [22] H. Baer, T. Barklow, K. Fujii, Y. Gao, A. Hoang, S. Kanemura, J. List, H. E. Logan, A. Nomerotski, M. Perelstein, et al., *The International Linear Collider Technical Design Report - Volume 2: Physics*, [arXiv:1306.6352](#).
- [23] **CEPC Study Group** Collaboration, M. Dong et al., *CEPC Conceptual Design Report: Volume 2 - Physics & Detector*, [arXiv:1811.10545](#).
- [24] **TLEP Design Study Working Group** Collaboration, M. Bicer et al., *First Look at the Physics Case of TLEP*, *JHEP* **01** (2014) 164, [[arXiv:1308.6176](#)].
- [25] **FCC** Collaboration, A. Abada et al., *FCC-ee: The Lepton Collider*, *Eur. Phys. J. ST* **228** (2019), no. 2 261–623.
- [26] L. Linssen, A. Miyamoto, M. Stanitzki, and H. Weerts, *Physics and Detectors at CLIC: CLIC Conceptual Design Report*, [arXiv:1202.5940](#).
- [27] **CLIC, CLICdp** Collaboration, P. Roloff, R. Franceschini, U. Schnoor, and A. Wulzer, *The Compact Linear e^+e^- Collider (CLIC): Physics Potential*, [arXiv:1812.07986](#).
- [28] A. Costantini, F. De Lillo, F. Maltoni, L. Mantani, O. Mattelaer, R. Ruiz, and X. Zhao, *Vector boson fusion at multi-TeV muon colliders*, 5, 2020. [arXiv:2005.10289](#).
- [29] C.-W. Chiang, X.-G. He, and G. Li, *Measuring the ratio of HWW and HZZ couplings through W^+W^-H production*, *JHEP* **08** (2018) 126, [[arXiv:1805.01689](#)].
- [30] Y. Chen, J. Lykken, M. Spiropulu, D. Stolarski, and R. Vega-Morales, *Golden Probe of Electroweak Symmetry Breaking*, *Phys. Rev. Lett.* **117** (2016), no. 24 241801, [[arXiv:1608.02159](#)].
- [31] **CMS** Collaboration, A. M. Sirunyan et al., *Measurements of properties of the Higgs boson decaying into the four-lepton final state in pp collisions at $\sqrt{s} = 13$ TeV*, *JHEP* **11** (2017) 047, [[arXiv:1706.09936](#)].
- [32] **ATLAS** Collaboration, M. Aaboud et al., *Measurement of inclusive and differential cross sections in the $H \rightarrow ZZ^* \rightarrow 4l$ decay channel in pp collisions at $\sqrt{s} = 13$ TeV with the ATLAS detector*, *JHEP* **10** (2017) 132, [[arXiv:1708.02810](#)].
- [33] **CMS** Collaboration, A. M. Sirunyan et al., *Measurements of properties of the Higgs boson decaying to a W boson pair in pp collisions at $\sqrt{s} = 13$ TeV*, *Phys. Lett.* **B791** (2019) 96, [[arXiv:1806.05246](#)].
- [34] **ATLAS** Collaboration, M. Aaboud et al., *Measurements of gluon-gluon fusion and vector-boson fusion Higgs boson production cross-sections in the $H \rightarrow WW^* \rightarrow e\nu\mu\nu$ decay channel in pp collisions at $\sqrt{s} = 13$ TeV with the ATLAS detector*, *Phys. Lett.* **B789** (2019) 508–529, [[arXiv:1808.09054](#)].
- [35] **ATLAS, CMS** Collaboration, G. Aad et al., *Measurements of the Higgs boson production and decay rates and constraints on its couplings from a combined ATLAS*

- and CMS analysis of the LHC pp collision data at $\sqrt{s} = 7$ and 8 TeV, *JHEP* **08** (2016) 045, [[arXiv:1606.02266](#)].
- [36] CMS Collaboration, A. M. Sirunyan et al., *Combined measurements of Higgs boson couplings in proton–proton collisions at $\sqrt{s} = 13$ TeV*, *Eur. Phys. J. C* **79** (2019), no. 5 421, [[arXiv:1809.10733](#)].
- [37] ATLAS Collaboration, G. Aad et al., *Combined measurements of Higgs boson production and decay using up to 80 fb⁻¹ of proton-proton collision data at $\sqrt{s} = 13$ TeV collected with the ATLAS experiment*, *Phys. Rev. D* **101** (2020), no. 1 012002, [[arXiv:1909.02845](#)].
- [38] M. Cepeda et al., *Report from Working Group 2: Higgs Physics at the HL-LHC and HE-LHC*, vol. 7, pp. 221–584. 12, 2019. [arXiv:1902.00134](#).
- [39] I. Low and J. Lykken, *Revealing the Electroweak Properties of a New Scalar Resonance*, *JHEP* **10** (2010) 053, [[arXiv:1005.0872](#)].
- [40] H. Georgi and M. Machacek, *DOUBLY CHARGED HIGGS BOSONS*, *Nucl. Phys.* **B262** (1985) 463–477.
- [41] J. Alwall, R. Frederix, S. Frixione, V. Hirschi, F. Maltoni, O. Mattelaer, H. S. Shao, T. Stelzer, P. Torrielli, and M. Zaro, *The automated computation of tree-level and next-to-leading order differential cross sections, and their matching to parton shower simulations*, *JHEP* **07** (2014) 079, [[arXiv:1405.0301](#)].
- [42] T. Sjostrand, S. Mrenna, and P. Z. Skands, *A Brief Introduction to PYTHIA 8.1*, *Comput. Phys. Commun.* **178** (2008) 852–867, [[arXiv:0710.3820](#)].
- [43] DELPHES 3 Collaboration, J. de Favereau, C. Delaere, P. Demin, A. Giammanco, V. Lemaître, A. Mertens, and M. Selvaggi, *DELPHES 3, A modular framework for fast simulation of a generic collider experiment*, *JHEP* **02** (2014) 057, [[arXiv:1307.6346](#)].
- [44] E. Leogrande, P. Roloff, U. Schnoor, and M. Weber, *A DELPHES card for the CLIC detector*, [arXiv:1909.12728](#).
- [45] A. Hoecker, P. Speckmayer, J. Stelzer, J. Therhaag, E. von Toerne, and H. Voss, *TMVA: Toolkit for Multivariate Data Analysis*, *PoS ACAT* (2007) 040, [[physics/0703039](#)].